X-rays at Sharp Focus: Chandra Science Symposium
*ASP Conference Series, Vol. **VOLUME**, 2002*
eds. S. Vrtilek, E. M. Schlegel, L. Kuhi

The 1 Ms Chandra Survey of the HDF-N: Populations at the Faintest X-ray Fluxes

ANN E. HORNSCHEMEIER
THE PENNSYLVANIA STATE UNIVERSITY, 525 DAVEY LAB, UNIVERSITY PARK, PA 16802

CDF-N TEAM
PSU, UH IFA, UW-MADISON, MIT CSR, CMU, CALTECH

Abstract. The Chandra Deep Field-North survey, which has at its center the Hubble Deep Field-North, has reached an exposure of 1 Ms and is now available to the public for analysis. This great astronomical resource will soon be released to the community in the form of a catalog paper with accurate X-ray fluxes in four bands and astrometry good to $\approx 0.6''$–$1.2''$ over the entire ACIS-I field.

The scientific focus of this contribution is the population of X-ray sources detected at X-ray fluxes below the faintest detection limits of X-ray observatories such as ROSAT and ASCA. These include fairly normal and star-forming galaxies out to $z \approx 2$, starburst galaxies from $z = 2$–4 and possibly very high redshift ($z > 6$) AGN. The exciting new prospects for studying these populations in the X-ray band are discussed.

1. Introduction: The Chandra Deep Field-North Survey

Our team is in the process of making an extremely deep survey of the Hubble Deep Field North (hereafter HDF-N) and its environs with the Advanced CCD Imaging Spectrometer on board the *Chandra X-ray Observatory*. This is one of the two deepest X-ray surveys ever performed; for point sources near the aim point it reaches 0.5–2.0 keV and 2–8 keV flux limits of $\approx 3 \times 10^{-17}$ erg cm^{-2} s^{-1} and $\approx 2 \times 10^{-16}$ erg cm^{-2} s^{-1}, respectively. Within the $\approx 20' \times 22'$ area (referred to as the Chandra Deep Field-North region, hereafter the "CDF-N"), 370 point sources and several extended sources are detected in the ACIS data. The 0.5–8 keV adaptively smoothed image of the field is shown in Figure 1. The detailed analysis of the CDF-N data is described in the catalog paper Brandt et al. (2001b; hereafter referred to as Paper V).

Figure 1 shows the outline of the HDF-N within the CDF-N, which comprises about 2% of the entire field. There are 15 X-ray sources detected in the this region (Paper V). These sources span a wide range of properties, with 0.5–2 keV rest frame luminosities between $\approx 2 \times 10^{39}$ erg s^{-1} and $\approx 5 \times 10^{44}$ erg s^{-1}, redshifts from $z = 0.089$ to $z = 3.479$, and a range of X-ray hardness ratios.

Figure 2 places the 1 Ms CDF-N survey into scientific perspective. Shown are a variety of 0.5–2 keV X-ray surveys (chosen to be representative, not com-

plete!). The flattening of the number counts is apparent as the net gain in number of sources per unit solid angle decreases at the faintest fluxes. One might find this flattening of the number counts discouraging, but in fact these faintest fluxes are quite tantalizing, for it is here that we reach the limits necessary to detect the most distant and most numerous classes of X-ray emitters.

The most distant are perhaps extreme redshift ($z > 6$) quasars, a population which was emitting X-rays very soon after the dawn of the modern Universe. These extremely distant objects are expected to be fairly optically faint, and studying them was one of the motivating factors for a comprehensive examination of optically faint ($I > 24$) sources within the CDF-N 1 Ms survey by Alexander et al. 2001 (hereafter Paper VI). A fair fraction of the X-ray background (15–30%) at the fainter flux levels is accounted for by these optically faint sources, and it is in this region of parameter space that one would expect $z > 6$ quasars to live.

The most numerous are "normal" galaxies where X-ray binaries, hot ISM, and supernovae contribute as much or more to the X-ray luminosity as accretion onto a nuclear black hole (Hornschemeier et al. 2001, hereafter Paper II and references therein; Brandt et al. 2001a, hereafter Paper IV). These sources typically have X-ray luminosities of 10^{39}–10^{41} erg s^{-1}, which can be reached to $z \approx 1$ in ≈ 1 Ms *Chandra* observations. It is predicted through modelling and through statistical analysis of the CDF-N data that the typical spiral galaxy will be detected in the 0.5–2 keV band at flux levels of $\approx 5 \times 10^{-18}$ erg cm^{-2} s^{-1} (Ptak et al. 2001; A. E. Hornschemeier et al., in prep; hereafter Paper VIII) and that normal galaxies will account for $\approx 5\%$ of the soft X-ray background.

In this contribution to the ASP Sharp Focus proceedings, I discuss both the optically faint (possibly $z > 6$) and the optically bright (low z normal galaxies) classes of X-ray sources, the reader is encouraged to consult the relevant CDF-N papers for more details.

Neither of these source populations (optically faint sources and "normal" galaxies) are particularly unexpected from an observational point of view. Most of the X-ray background flux is explained by active galaxies, which have been observed to typically exist within a well-defined range of X-ray-to-optical flux ratios (Schmidt et al. 1998). Thus, if one extends this trend to faint X-ray fluxes, the optical counterparts predicted are indeed quite optically faint (see Figure 3). Below 0.5–2 keV fluxes of $\approx 1 \times 10^{-15}$ erg cm^{-2} s^{-1}, a source population is seen to arise with X-ray-to-optical flux ratios lower than typically seen in AGN populations, this is simply due to the flux limits being sufficiently low to detect non-AGN activity at low-to-moderate redshift ($z < 1$).

2. Optically Faint ($I > 24$) X-ray Sources

A detailed analysis of optically faint ($I \geq 24$) X-ray sources identified within the 1 Ms CDF-N exposure has been made in Paper VI. In this paper, we studied an $8.4' \times 8.4'$ region within the Hawaii flanking-field area containing the Hubble Deep Field North region. Analysis of the optical and X-ray properties suggests a large number of these optically faint X-ray sources are likely to host obscured AGN activity at $z = 1$–3 (Paper VI).

Figure 1. Adaptively smoothed image of the CDF-N in the 0.5–8 keV band. This image has been binned by a factor of four in both right ascension and declination. The adaptive smoothing has been performed using the code of Ebeling, White, & Rangarajan (2001) at the 2.5σ level. Much of the apparent diffuse emission is instrumental background. The light colored grooves running through the images correspond to the gaps between the CCDs. The small polygon indicates the HDF-N itself.

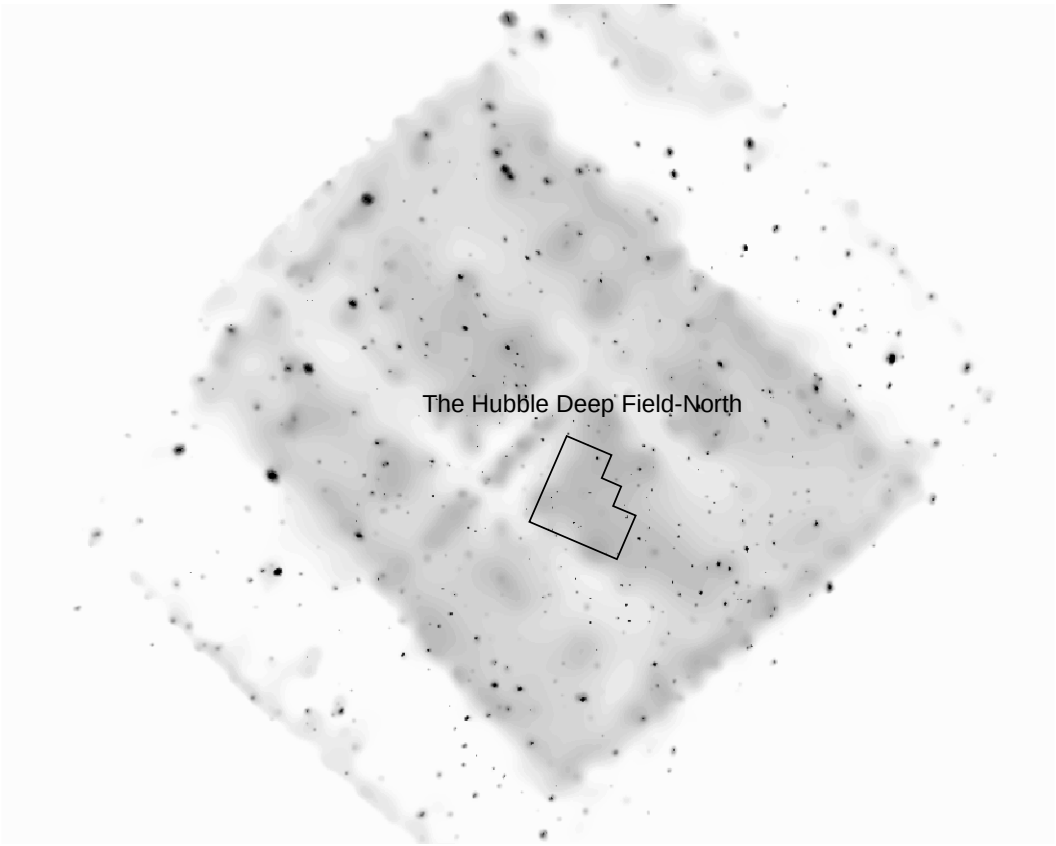

Figure 2. Distribution of some extragalactic X-ray surveys in the 0.5–2.0 keV flux limit versus solid angle plane, adapted from Paper V. Shown are the *Uhuru* survey (e.g., Forman et al. 1978), the *ROSAT* All-Sky Survey (RASS; e.g., Voges et al. 1999), the *Einstein* Extended Medium-Sensitivity Survey (EMSS; e.g., Gioia et al. 1990), the *ROSAT* International X-ray/Optical Survey (RIXOS; e.g., Mason et al. 2000), the *XMM* Serendipitious Surveys (*XMM* Bright, *XMM* Medium, *XMM* Faint; e.g., Watson et al. 2001) , the *Chandra* Multiwavelength Project (ChaMP; e.g., Wilkes et al. 2001), the *ROSAT* Ultra Deep Survey (UDS; e.g., Lehmann et al. 2001), the deep survey of the Lockman Hole (*XMM* LH; e.g., Hasinger et al. 2001), *Chandra* 100 ks surveys (e.g., Mushotzky et al. 2000), and *Chandra* 1 Ms surveys (i.e., the current one and the *Chandra* Deep Field South survey, see Colin Norman's CDF-S contribution to these proceedings) Solid dots are for surveys that have been completed, and open circles are for surveys that are in progress. The dotted curves show, from top to bottom, the loci of 100, 1000, and 10000 0.5–2.0 keV sources (these have been calculated using the number counts of Hasinger et al. 1998 and Garmire et al. (2001; Paper III); for example, a 1 degree^2 survey with a 0.5–2.0 keV flux limit of 9.5×10^{-15} erg cm^{-2} s^{-1} will detect ≈ 100 sources.

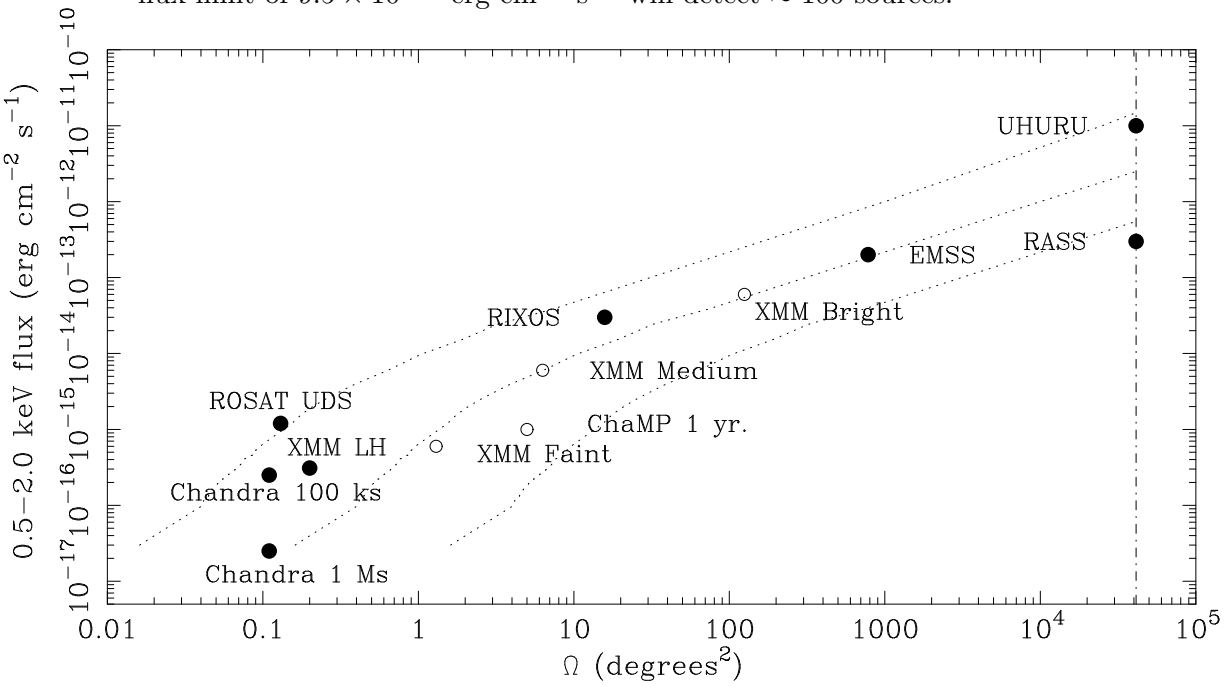

Figure 3. Plot of R magnitude versus 0.5–2 keV flux for X-ray detected sources, adapted from Paper II. Solid triangles are sources from the CDF-N data of Paper II, and open circles are those from Mushotzky et al. (2000). Solid dots are sources from Schmidt et al. (1998). We plot only the AGN from Schmidt et al. (1998). The two stars are spectroscopically identified stars The vertical dotted lines show the Paper II detection limits for an assumed $\Gamma = 1.4$ power-law spectrum; sources slightly beyond these lines have spectral shapes differing from a $\Gamma = 1.4$ power law. The boxes mark our sources with extreme $\log\left(\frac{f_{\rm X}}{f_{\rm R}}\right)$ values.

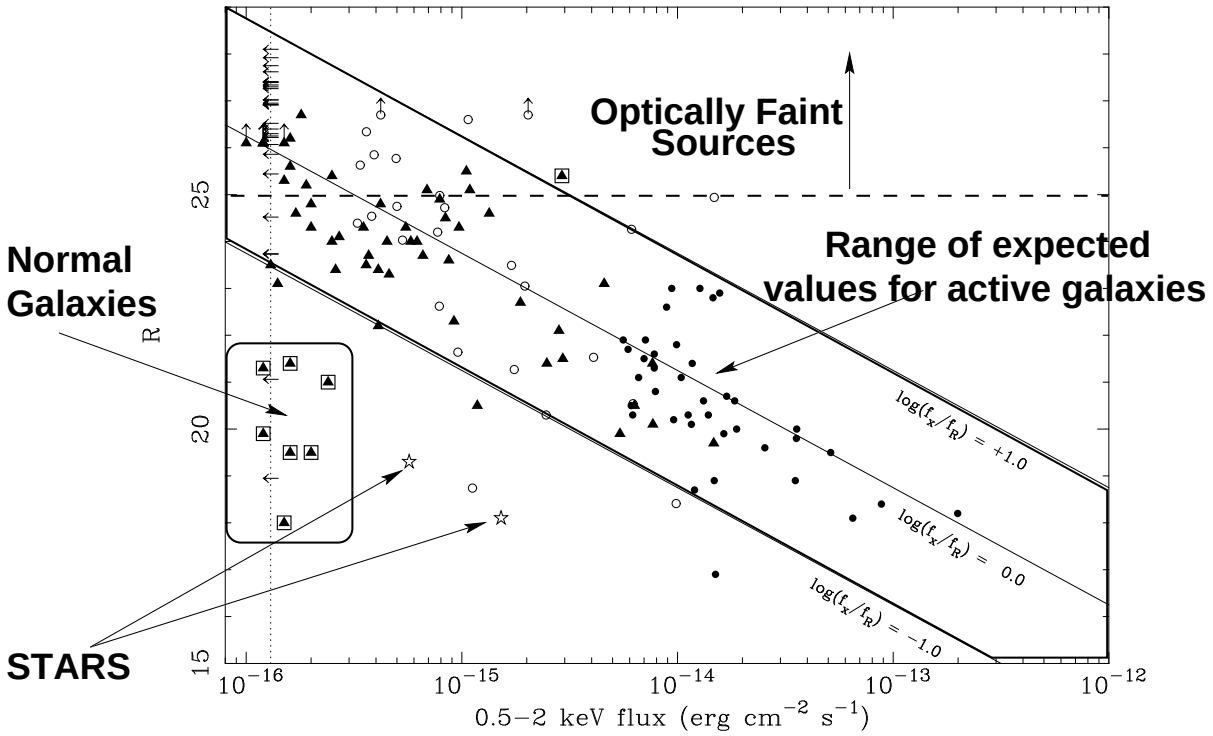

The X-ray flux distribution of the optically faint sources is consistent with that of the optically bright source population, indicating that this population does not suddenly arise below some faint X-ray flux level. Their X-ray-to-optical flux ratios are consistent with AGN in the local Universe (see Figure 3). Their fairly red optical colors are not consistent with these objects being unobscured broad-line AGN and, as a population, they have flatter X-ray slopes on average than the optically bright sources (Paper VI). Note that while *on average* they are X-ray harder, they are not all X-ray hard; there is at least one apparently normal broad-line AGN within the optically faint CDF-N population studied in Paper VI. However, the majority of the optically faint X-ray sources are consistent with being obscured AGN (Paper VI).

Obscured AGN have their optical emission dominated in most cases by the host galaxy and this property can be used to place constraints on source redshifts. In Figure 4 (adapted from Paper VI), SED tracks of I-band magnitude vs. redshift are plotted, showing the way in which different classes of objects become fainter at increasing redshift. We expect that obscured AGN and fairly normal galaxies will follow the SED tracks for the Sc, Sa, or E type galaxies rather than the QSO SED. Overplotted are the data showing the average spectroscopic redshifts for the optically bright population, excluding the confirmed broad-line AGN: these X-ray sources do indeed follow the SED tracks of normal galaxies. One can then extend these tracks to fainter optical magnitudes to place some constraints on their redshifts. It is found that for $I > 24$, one expects the objects to have $z = 1$–3. For the few optically faint sources with either photometric or spectroscopic redshifts, this appears to hold reasonably well (Paper VI).

Extreme redshift QSOs ($z > 6$) would not only be optically faint but "optically blank" even in the very deep ($I \approx 25.3$) optical imaging data of the CDF-N due to the Lyman break entering the I-band at $z \approx 6$. Within the area under study in Paper VI, there were only 15 sources having no counterparts down to $I \approx 25.3$ ($\approx 10\%$ of the sources). Based on a simple hierarchial cold dark matter model and using constraints from the QSO X-ray luminosity function, Haiman & Loeb (1999) predicted $\approx$ 15 QSOs (i.e., $L_X > 10^{44}$ erg s^{-1}) at $z > 6$ at the depth and area of our survey. While this is comparable to the number of optically blank sources detected, for several reasons described in Paper VI, it is likely that most of the optically blank X-ray sources lie at similar redshifts to the optically faint X-ray sources and hence at $z < 6$. We are thus placing the first significant constraints on this population and are currently not finding evidence for a large population of extremely high redshift AGN.

3. Optically Bright X-ray Sources: Constraints on Normal Galaxies

3.1. Galaxies at $0.3 < z < 2.0$: Probing the X-ray Response to the Star-Formation Peak

The CDF-N has reached the depths necessary to detect fairly normal galaxies to $z \approx 0.3$ (see Figure 5 for an example), or look-back times of several Gyr. Although these normal galaxies comprise only 10–15% of the soft-band sources in the CDF-N survey, it is expected that they will dominate the number counts at 0.5–2 keV fluxes of $\approx 1\times10^{-17}$–1×10^{-18} erg cm^{-2} s^{-1} (Ptak et al. 2001). The

Figure 4. I-band vs. z tracks for different SEDs with CDF-N data overplotted, (adapted from Paper VI). The filled triangles are the broad-line AGN, the filled squares are the luminous narrow-line AGN, the open circles are optically faint X-ray sources with spectroscopic or photometric redshifts. The filled circles are the average spectroscopic redshifts for the $I < 23$ *Chandra* sources. The crosses are the average photometric redshifts for optical sources in the HDF-N (from Fernández-Soto, Lanzetta, & Yahil 1999). The solid, long-dashed and short-dashed curves are the redshift tracks of $M_I = -23$ E, Sa and Sc host galaxies. The dotted curve is the redshift track of an $M_I = -23$ QSO (for details on these calculations, see Paper VI). This figure suggests that if the optically faint X-ray sources are the high-redshift analogs of the optically bright X-ray sources, the majority should lie at $z \approx 1$–3.

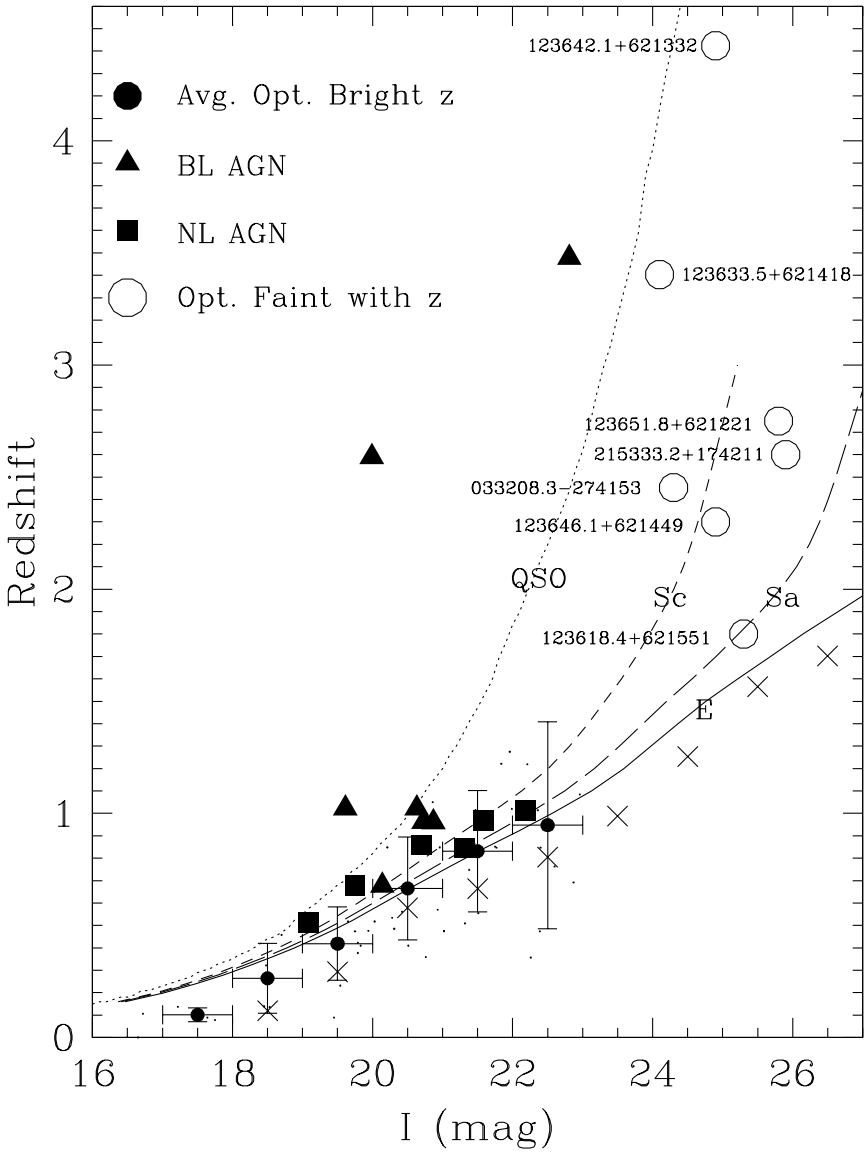

emission mechanisms in the galaxies detected thus far are quite diverse: several are dominated by ultra-luminous off-nuclear X-ray sources which are most likely binaries, other show signs of being low-luminosity AGN, whereas the typical galaxy has an X-ray hardness ratio consistent with binary populations (Paper II; Tozzi et al. 2001; A.E. Hornschemeier et al., in preparation).

It is expected that the X-ray luminosity per unit B-band luminosity for normal galaxies will increase at $z \approx 0.5$–1 due to the production of X-ray binaries from $z \approx 1$–3 (e.g., Ghosh & White 2001; Ptak et al. 2001). It is possible to test this expectation despite the anticipated extremely faint X-ray flux of the typical galaxy by stacking the data from individually undetected galaxies. We have empirically assessed the stacking false-detection probabilities by performing Monte-Carlo simulations designed to reproduce the actual stacking as closely as possible. Figure 6 shows an example of 100,000 such trials, the resulting distribution is closely Gaussian and this particular stacking result was expected for less than 1 of those 100,000 trials, indicating a highly significant (i.e., 99.999% confidence) average detection (see Paper IV for more details).

These stacking analyses have allowed us to study samples of spiral galaxies within the HDF-N and its environs; we have found the typical spiral galaxy is detected at 0.5–2 keV X-ray fluxes of $\approx(3$–$5)\times10^{-18}$ erg cm^{-2} s^{-1} (Paper VIII). The X-ray to B-band luminosity ratios, which indicate the level of current and recent star-formation activity in a normal galaxy, are found to not evolve upwards by more than a factor of ≈ 2 to $z \approx 1$ (Paper IV, Paper VIII) but some upwards evolution is detected by $z \approx 2$. Since different global star-formation rates can lead to very different X-ray luminosity evolution profiles (e.g. Ghosh & White 2001), these constraints on evolution of galaxies in the X-ray band are a useful independent probe of the cosmic star-formation history. For more details, please see Paper VIII.

3.2. Galaxies at $2 < z < 4$: Lyman Break Galaxies

Over the last few years, the Lyman break technique has been used extensively to isolate galaxies at $z \approx 2$–4 (e.g., Steidel et al. 1996; Lowenthal et al. 1997; Dickinson 1998) and hence observe activity near the peak of the cosmic star-formation rate (e.g., Blain et al. 1999). Lyman break galaxies often exhibit stellar and interstellar absorption lines characteristic of local starburst galaxies, and have B-band luminosities somewhat larger than present-day L^*. Their morphologies are varied, with multiple knots of emission and diffuse wispy tails that suggest nonrelaxed systems.

We selected galaxies within the HDF-N with z =2–4 for stacking analysis using the available spectroscopic redshift catalogs (e.g. Cohen et al. 2000; see references in Paper VII); there are 28 such objects, and most were found using the Lyman break technique (the *HST* U_{300} filter has allowed Lyman break galaxies to be found down to $z \approx 2$ in the HDF-N; e.g., Dickinson 1998). The stacked images have effective exposure times of 22.4 Ms (260 days) and the average rest-frame 2–8 keV luminosity of a Lyman break galaxy is derived to be $\approx 3.2 \times 10^{41}$ erg s^{-1}, comparable to that of the most X-ray luminous starbursts in the local Universe. The observed ratio of X-ray to B-band luminosity is consistent with that seen from local starbursts. The X-ray emission probably

Figure 5. An X-ray detected normal galaxy at $z \approx 0.1$ in the CDF-N (A.E. Hornschemeier et al., in preparation). The X-ray source is $\approx 3.0''$ from the galaxy's nucleus and has an X-ray luminosity of $\approx 2 \times 10^{39}$ erg s^{-1}. It is coincident with a knot on one of the spiral arms of the galaxy and is most likely a super-Eddington X-ray binary system or starburst region. This cut-out is from a deep V image that covers the entire CDF-N field (see A. Barger et al., in preparation for more information on the deep optical image).

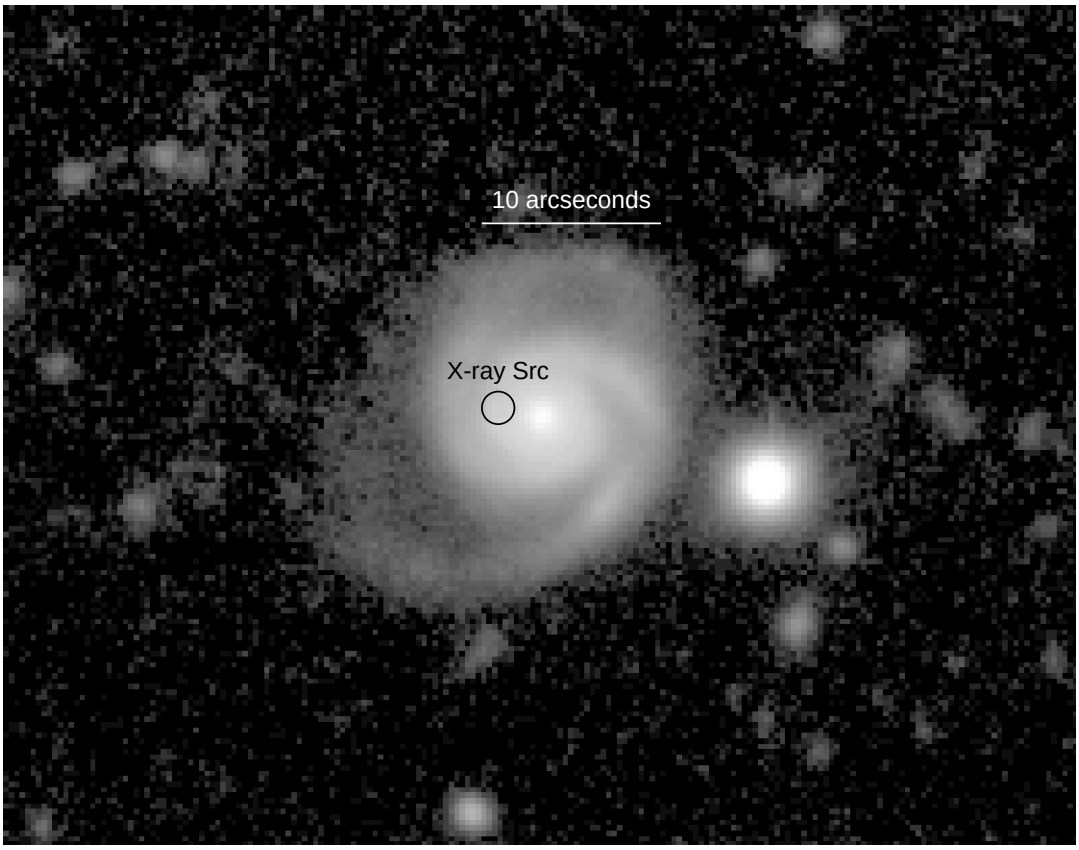

Figure 6. Results from the Monte-Carlo testing of the galaxy stacking analysis. We performed 100,000 stacking trials at randomly selected positions, and plotted the number of trials yielding a given number of counts in the stacking aperture (see Paper IV for a more detailed description). The arrow indicates the number of counts obtained for the galaxies of interest; the detection is significant at the $> 99.99\%$ level.

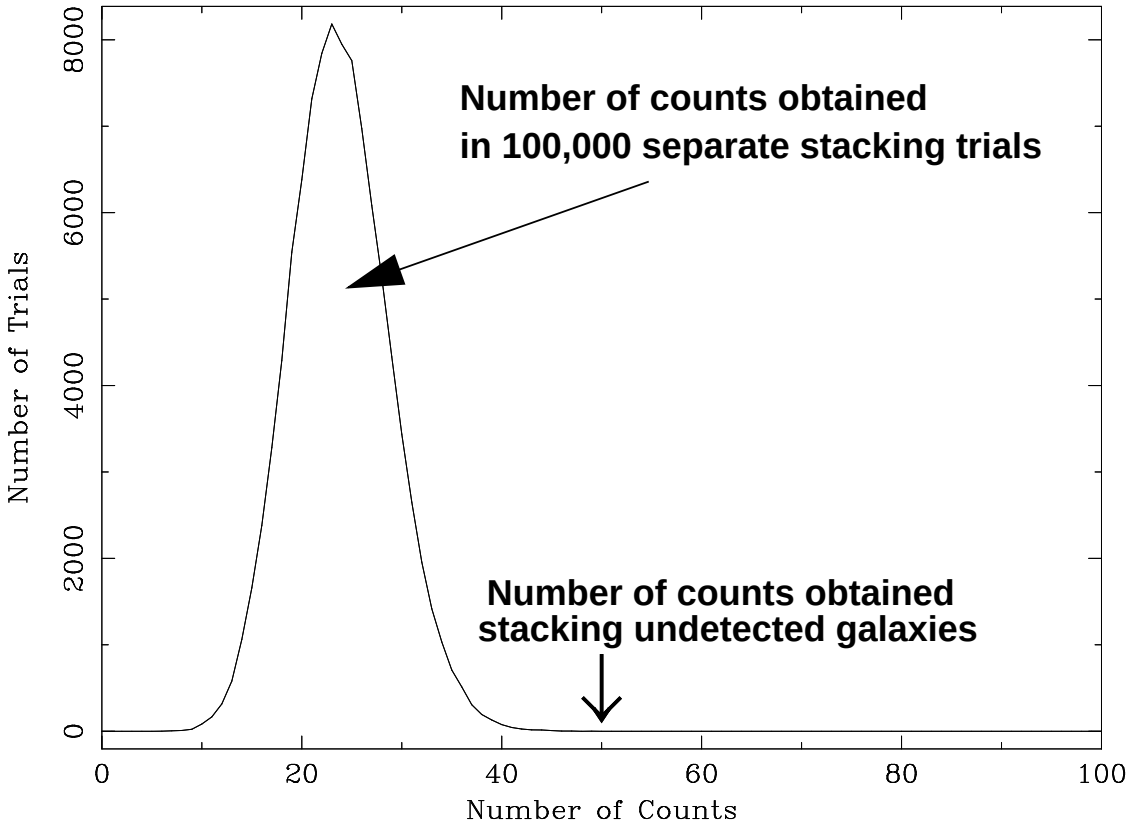

arises from a combination of high-mass X-ray binaries, "super-Eddington" X-ray sources, and low-luminosity active galactic nuclei (see Paper VII).

4. The Future

Members of the CDF-N team (A. Barger and L. Cowie) are obtaining extremely deep wide-field optical and near-infrared coverage and will be able to further the analysis performed in Paper VI. The optically faint X-ray source population should be better constrained by using the properties of the multi-band optical photometry to obtain photometric redshifts.

The stacking results show that *Chandra* ACIS performs well at source detection even with effective exposure times of 260 days. Any systematic effects that cause the sensitivity to deviate from that expected by photon statistics appear mild. Stacking analyses using deeper observations with *Chandra* will allow this work to be extended.

The CDF-N survey will go to 2 Ms of coverage over the course of the next year and the ultimate goal is to obtain 5 Ms of coverage over the next ≈ 5 years. This is an ambitious project and will fulfill one of *Chandra's* central design goals and become a long-lasting (≈ 20 year) legacy of *Chandra*, laying the groundwork for the next generation of X-ray telescopes. *XEUS* and *Generation-X* are designed to detect sources to $\sim 10^{-18}$ erg cm^{-2} s^{-1} and perform X-ray spectroscopy on sources to $\sim 10^{-17}$ erg cm^{-2} s^{-1}. A 5 Ms *Chandra* observation will detect sources to $\approx 10^{-17}$ erg cm^{-2} s^{-1}. These observations will bolster the scientific cases for these missions, not due to be operational for 15–20 years, and will be invaluable when planning their design.

References

Alexander, D.M. , Brandt, W.N., Hornschemeier, A.E., et al., 2001, AJ, in press (Paper VI; astro-ph/0107450)

Blain, A.W., Smail, I., Ivison, R.J., & Kneib, J.-P. 1999, MNRAS, 302, 632

Brandt, W.N., et al. 2000, AJ, 119, 2349

Brandt, W.N., Hornschemeier, A.E., Alexander, D.M. et al. 2001a, AJ, 122, 1 (Paper IV)

Brandt, W.N., Alexander, D.M., Hornschemeier, A.E., et al., 2001b, AJ, submitted (Paper V)

Brandt, W.N., Hornschemeier, A.E., Schneider, D.P. et al., 2001c, AJ, in press (Paper VII; astro-ph/0107392)

Cohen, J.G., Hogg, D.W., Blandford, R., Cowie, L.L., Hu, E., Songaila, A., Shopbell, P., & Richberg, K. 2000, ApJ, 538, 29 (C00)

Cowie, L.L., et al. 2001, ApJ, 551, L9

Dickinson, M. 1998, in The Hubble Deep Field, eds. Livio, M., Fall, S.M., & Madau, P. (Cambridge University Press, Cambridge), p. 219

Ebeling, H., White, D.A., & Rangarajan, F.V.N. 2001, MNRAS, submitted

Forman, W., Jones, C., Cominsky, L., Julien, P., Murray, S., Peters, G., Tananbaum, H., & Giacconi, R. 1978, ApJS, 38, 357

Garmire, G.P., et al. 2001, ApJ, submitted (Paper III)

Ghosh, P. & White, N., ApJ, in press

Giacconi, R., et al. 2001, ApJ, in press (astro-ph/0007240) (G01)

Gioia, I., Maccacaro, T., Schild, R., Wolter, A., Stocke, J., Morris, S., & Henry, J.P. 1990, ApJS, 72, 567

Haiman, Z., & Loeb, A. 1999, ApJ, 521, L9

Hasinger, G., et al. 1998, A&A, 340, L27

Hasinger, G., et al. 2001, A&A, 365, L45

Hornschemeier, A.E., Brandt, W.N., Garmire, G.P., Schneider, D.P., et al. 2001a, ApJ, 554, 742 (Paper II)

Lehmann, I., et al. 2001, A&A, 371, 833

Lowenthal, J.D., et al. 1997, ApJ, 481, 673

Mason, K.O., et al. 2000, MNRAS, 311, 456

Mushotzky, R.F., Cowie, L.L., Barger, A.J., & Arnaud, K.A. 2000, Nature, 404, 459

Ptak, A. et al. 2001, ApJ, submitted

Schmidt, M., Hasinger, G., Gunn, J., Schneider, D., Burg, R., Giacconi, R., Lehmann, I., MacKenty, J., Trümper, J., & Zamorani, G. 1998, A&A, 329, 495

Steidel, C.C., Giavalisco, M., Pettini, M., Dickinson, M., & Adelberger, K.L. 1996, ApJ, 462, L17

Tozzi, P., et al. 2001, ApJ, in press (astro-ph/0103014)

Watson, M.G., et al. 2001, A&A, 365, L51

Wilkes, B.J., et al. 2001, in Proceedings of the New Era of Wide Field Astronomy, eds. Clowes, R.G., Adamson, A.J., & Bromage, G.E. (ASP Press, San Francisco), in press (astro-ph/0011377)

Voges, W., et al. 1999, A&A, 349, 389